Analysis and Implementation of Two Phase Flux Reversal Free Doubly Salient Machine

Prabhu Sundaramoorthy[1]* and Balaji Mahadevan[2]

[1]*Department of Electrical and Electronics Engineering, Arunai Engineering College, Tiruvannamalai, India*
[2]*Department of Electrical and Electronics Engineering, SSN College of Engineering, Chennai, India*

The major factors that limit the application prospects of Switched Reluctance Motor (SRM) include torque ripple, noise and vibration. The main reason attributed to these drawbacks is the nature of flux linkage variation in accordance with rotor position. In this aspect this work analyses the effect of embedding permanent magnets in the stator and the impact of their orientation on the flux linkage characteristics and hence on the performance of the motor. In addition the effect of lamination material on the characteristics of the motor is analysed. The materials considered include M850-65A, M-19, M-43, Pure Soft Iron, and M800-50D. This paper proposes, the optimization of Permanent Magnet Flux Reversal Free Switched Reluctance Motor (PMFRFSRM) through the orientation of permanent magnets and choice of suitable laminating materials to improve the performance characteristics of the motor. The analysis is performed using Finite Element Analysis (FEA) based package MagNet and the results are validated with hardware prototype.

Keywords : Flux Density, M800-65A, M-19, M-43, Pure Soft Iron, M890-50D

1. Introduction

PMFRFSRM is a type of reluctance torque machine. To increase the air gap flux density permanent magnet (PM) is inserted into the shared pole of stator producing permanent flux and the windings in the main pole develop electromagnetic flux. These two fluxes aid together to increase the air gap flux. These PM contribute to the cogging torque in addition to the inherent torque ripple in the motor. To mitigate the problems the effect of modified pole shapes have been analysed [1-3].

$$\lambda = Li \qquad (1)$$

λ : Flux Linkage
i : Current

In this article the technique for minimizing the torque ripple and increasing the flux density in the air gap with FRFSRM is initiated as follows. Firstly, FRFSRM is modelled and analyzed with FEA to plot the reluctance, cogging torque and flux linkage characteristics with respect to rotation angle [4-6]. Secondly, the increase in air gap flux density is analysed by orienting the magnets on the main poles (PM-MP), inter-linking the magnets between stator poles (PM-ILSP) and circular assist PM (PM-CSP). The performance is analysed with respect to the flux linkage and torque characteristics. Finally the performance of the motor with various laminating steel material are investigated and the experimental results are presented.

2. Modelling of Permanent Magnet FRFSRM

The torque in PMFRFSRM is due to the reluctance variation and the presence of magnet in the main and auxiliary poles respectively [7-9]. A motor with 10 rotor poles, with stator arranged as an E-Core structure as shown in Fig. 1. The structure of PMFRFSRM is derived from the E-Core structure with permanent magnets embedded in the stator as shown in Fig. 2. The dimensions of the motor considered in this work is given in appendix 1. PM is inserted in the auxiliary or shared pole at the inner periphery of the stator. Figure 3 plots the B-H curve of cold rolled steel. Presence of PM in E-Core SRM contributes to the cogging torque.

*Corresponding author: Tel: +91 9600646211
Fax: 04142 237789, e-mail: prabhuphd1987@gmail.com
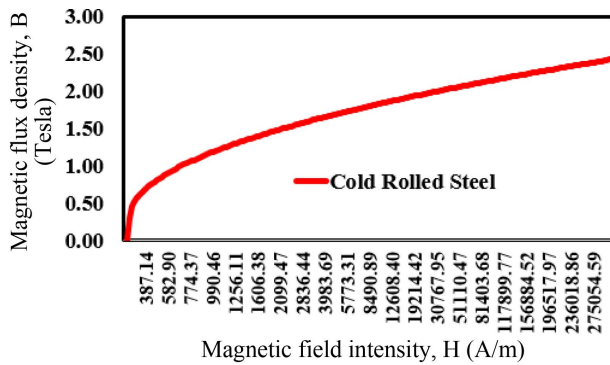
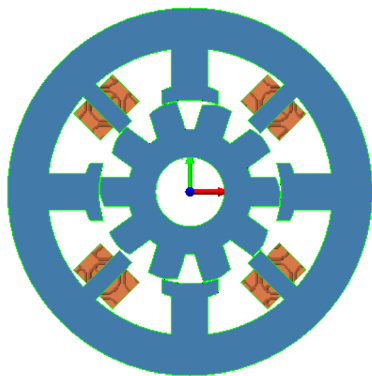**Fig. 1.** (Color online) B-H Curve of Cold Rolled Steel.

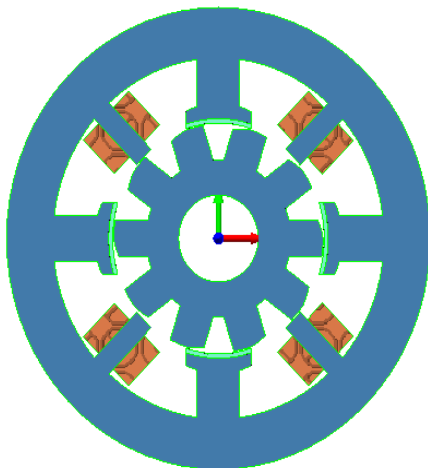**Fig. 2.** (Color online) E-Core SRM.

Fig. 3. (Color online) PMFRFSRM.

The rotor position is illustrated by, [10-12]

$$\theta = \frac{360}{Q * N_r} \qquad (2)$$

Step Angle of Rotor,

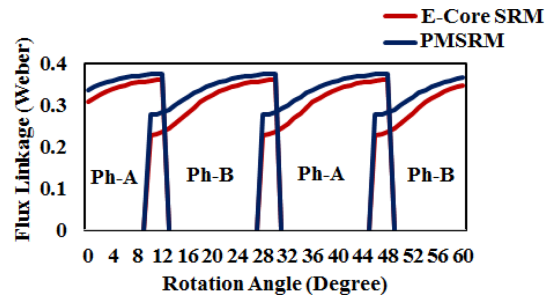Q : Number of phases
N_r : Number of rotor poles

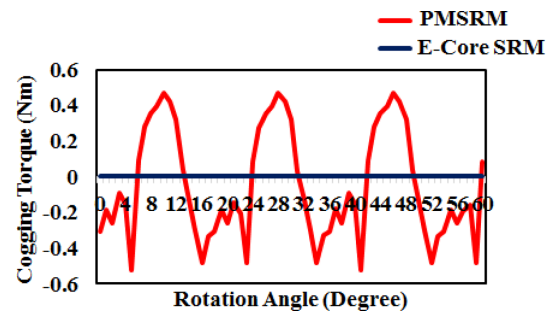**Fig. 4.** (Color online) Flux Linkage vs Rotation Angle.

Fig. 5. (Color online) Cogging Torque vs Rotation Angle.
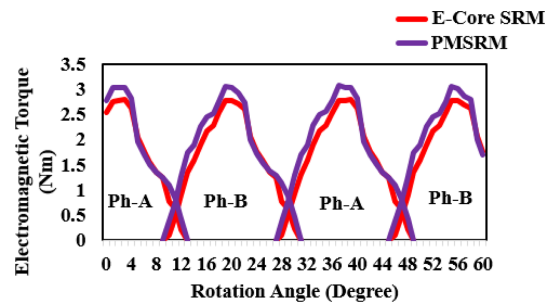

Fig. 6. (Color online) Electromagnetic Torque vs Rotation Angle.

The reluctance and magnet component aid each other to increase the average torque and flux density at the air gap. Figure 4 explains the variation of flux linkage in the E-Core structure and PMFRFSRM. From the figure it is evident that the presence of permanent magnet improves the flux linkage characteristics. The variation of cogging torque with respect to rotation angle is shown in Fig. 5. Due to the absence of PM in E-Core SRM, there is no cogging torque. The static electromagnetic torque of the motor is depicted in Fig. 6. and it is evident that the PMFRFSRM produces higher torque. The flux density distribution of E-Core and PMFRFSRM is illustrated in Fig. 7 and Fig. 8 respectively. Table 1 compares the torque ripple and magnetic properties of E-Core SRM and PMSRM, to infer that the magnetic properties of PMFRFSRM seems to be better than E-Core SRM.
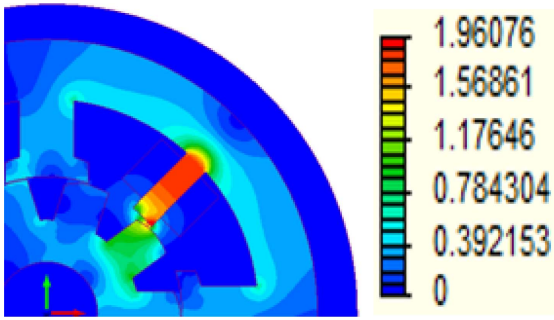
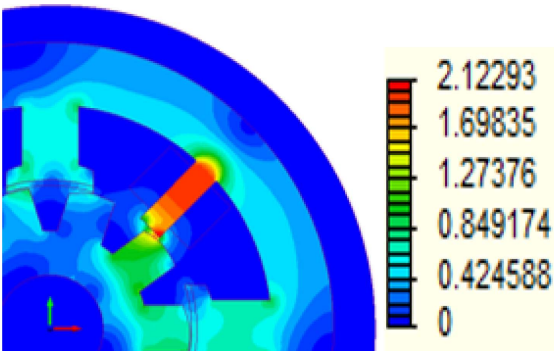**Fig. 7.** (Color online) Flux Density Distribution.

Fig. 8. (Color online) Flux Density Distribution.

The flux linkages are able to be estimated by investing with partial derivatives as, [13-16],

$$v = R_s i + \frac{d\lambda(\theta, i)}{dt} \tag{3}$$

$$p\lambda(\theta, i) = L(\theta, i)_{\theta=cons\tan t} \frac{di}{dt} + i \frac{dL(\theta, i)}{dt}_{i=cons\tan t} \tag{4}$$

p is the operator of derivative, $\frac{d}{dt}$

2.1. Orientation of PM in SRM

The placement and orientation of permanent magnets in the stator pole is bound to alter the performance charac-
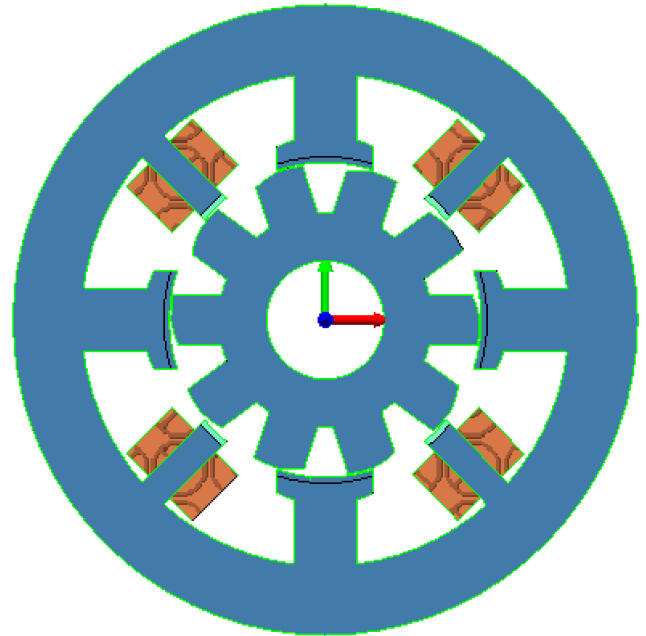

Fig. 9. (Color online) PM Assists Main Pole SRM.

teristics of the motor. In this aspect the following orientation schemes are analysed in this work

　a. PM assists Main pole (PM-MP)
　b. PM assists inter-linked stator pole (PM-ILSP)
　c. PM assists circular Stator Pole (PM-CSP)

a. PM Assists Main Poles

In the PM-MP configuration there is significant reduction in flux density due to the opposition caused by the placement of magnets and windings in the main poles. So the flux density distribution in the air gap of the machine reduces to 0.83T. Figure 9 and Fig. 10 displays the pictorial representation of PM assists main pole SRM and the flux density distribution of PM respectively.

b. PM Assists inter-linked stator poles

In PM-ILSP, the active region is increased due to the influence of PM connecting the main and auxiliary pole.

Table 1. Comparison of E-Core and PMFRFSRM.

| Parameters/Machine	E-Core SRM	PMFRFSRM
Torque Ripple (Nm)	1.265	1.106
Air gap Flux Density due to main poles (Tesla)	0.451	1.740
Air gap Flux Density due to Shared Poles (Tesla)	0.151	1.573
Flux density at main poles (Tesla)	1.891	2.232
Flux Density at shared poles (Tesla)	0.406	0.652
Flux Density at Stator Back Iron (Tesla)	0.419	0.483
Flux Density at Rotor Poles (Tesla)	1.588	1.957
Flux Density at Rotor Back Iron (Tesla)	0.536	0.602
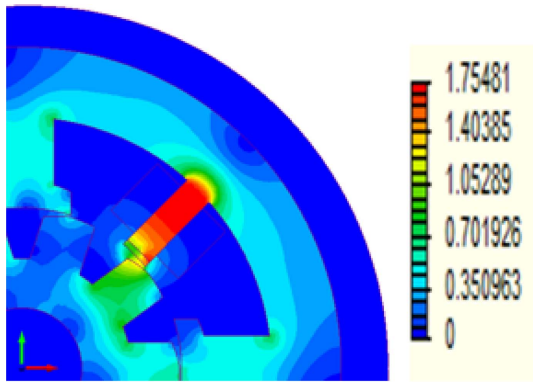
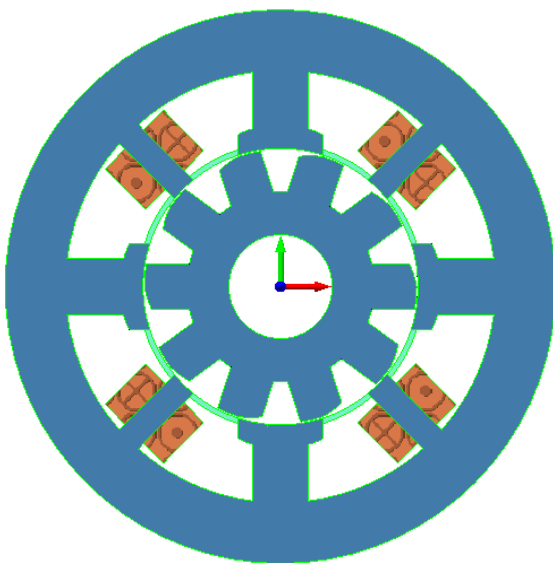**Fig. 10.** (Color online) Flux Density Distribution of PM-MP.

Fig. 11. (Color online) PM Assists inter-linked stator pole SRM.
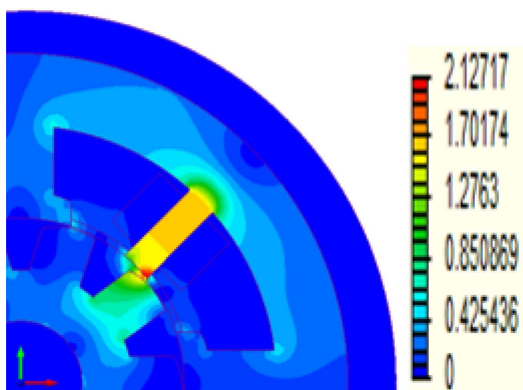

Fig. 12. (Color online) Flux Density Distribution of PM-ILSP.

This arrangement increases the flux density and hence average torque. Such arrangement indirectly increases the stator pole arc thereby increasing the average torque. The
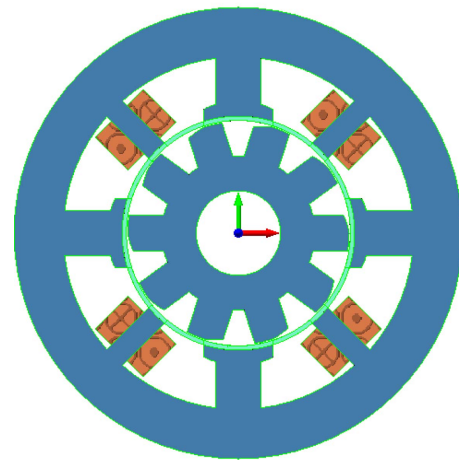

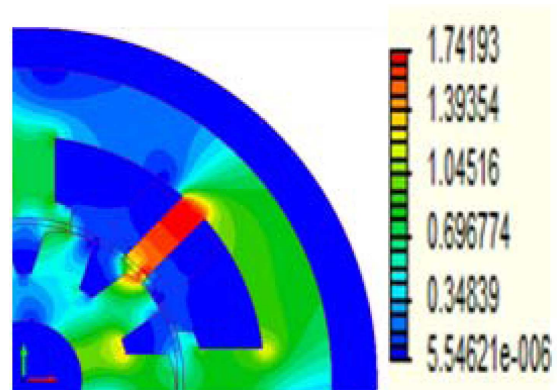**Fig. 13.** (Color online) PM Assists Circular (Short- Circuited) SRM.

Fig. 14. (Color online) Flux Density Distribution of PM-CSP.

air gap flux density increases to 2.1T. Figure 11 and Fig. 12 shows the diagrammatic representation of PM-ILSP and its flux distribution respectively.

c. PM Assists Circular Stator Poles

PM-CSP configuration is shown in Fig. 13. In PM-CSP all main and auxiliary pole are connected together through the magnet. The air gap flux density reduces to 1.745T while cogging torque increases to 1.1 Nm. The flux distribution of this configuration is shown in Fig. 14.

2.1.1. FEA inference with PM Orientation in SRM

The comparison of cogging torque of PM-MP, PM-ILSP and PM-CSP configurations are shown in Fig. 15 and from the figure it is evident that the cogging torque of PM-ILSP configuration is less. Figure 16 and Fig. 17 depicts the electromagnetic torque and flux linkage characteristics of various configurations to illustrate the fact that PM-ILSP configuration produces higher torque.
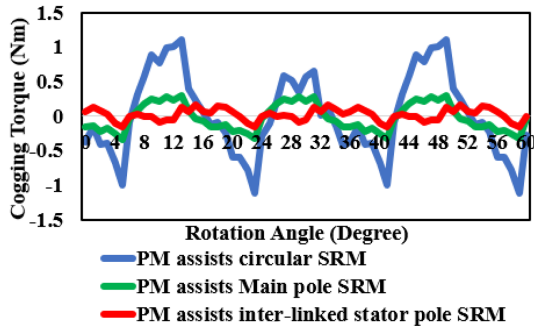
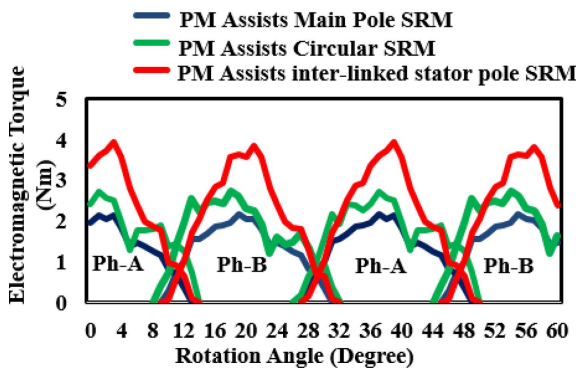**Fig. 15.** (Color online) Cogging torque profile of PM orientated SRM.

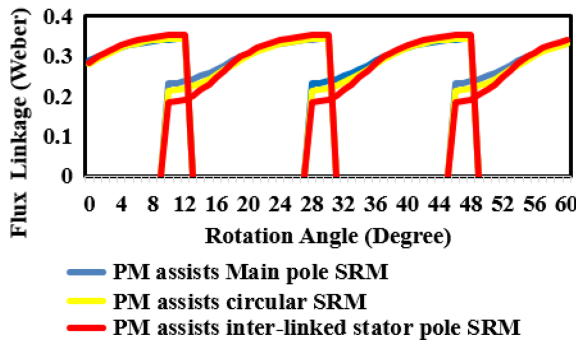**Fig. 16.** (Color online) Electromagnetic Torque for PM orientated SRM.

Fig. 17. (Color online) Flux linkages for PM orientated SRM.

Table 2. Comparison of orientation of PM in SRM.

Parameters (Nm)	PM-CSP	PM-MP	PM-ILSP
Cogging Torque	1.18	0.3	0.17
Maximum Torque	2.714	2.15	3.93
Minimum Torque	1.4	0.75	0.859
Average Torque	1.898	1.504	2.279
Torque Ripple	0.692	0.933	1.348

A complete analysis of the performance characteristics is presented in Table 2 and the entries in table illustrate that the PM-ILSP configuration outperforms the other
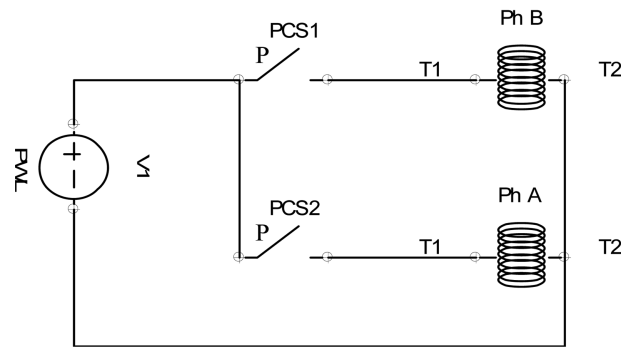

Fig. 18. (Color online) Equivalent driver circuit for PM-ILSP SRM.
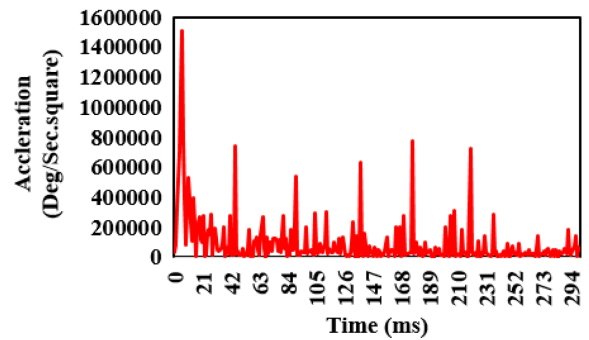
Fig. 19. (Color online) Acceleration of PM-ILSP SRM.
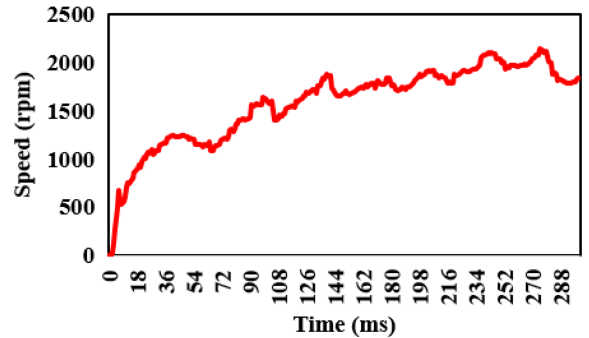
Fig. 20. (Color online) Speed in rpm of PM-ILSP SRM.

configurations. The dynamic characteristics are obtained using circuit coupled simulation with the driver circuit as depicted in Fig. 18. The acceleration and speed characteristics of the PM-ILSP is illustrated in Fig. 19 and 20 respectively.

3. Electromagnetic Material Optimization

The core loss of reluctance motor depends on the flux density and permeability of material. The precise estimation of core loss provides a path to improve the performance of reluctance motor [17]. The core loss of the motor depends on the material and the choice of material

Fig. 21. (Color online) B-H Characteristics of M43, Pure soft Iron, M890-50D, M19 steel.

Fig. 22. (Color online) Core Loss Curves of M800-65A, M890-50D, M-43, Pure Soft Iron, M-19 at 50 Hz.

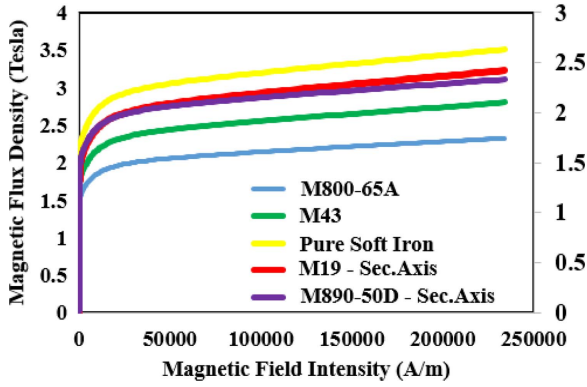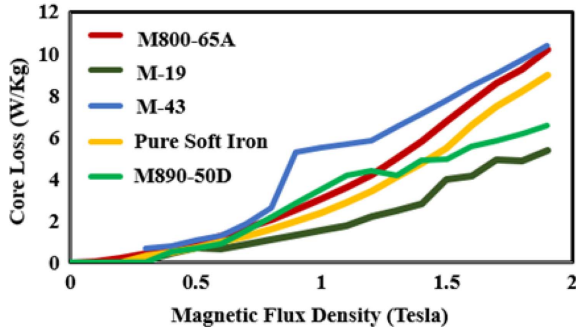plays a vital role in enhancing the performance of the motor. Figure 21. compares the B-H characteristics of the different laminating material namely M-43, M800-65A, pure soft iron, M-19, M890-50D with secondary axis. The comparison of core loss curves are presented in Fig. 22. From the figure it is evident that the core loss of M890-50D is less by 54.54 % while the core loss of M800-65A is less by 9.09 % in comparison with M-43 laminating Steels. The magnetic and material properties of core materials are tabled in Table 3. The investigation of torque characteristics is preferred with M800-65A as illustrated in Table 4.

Table 3. Magnetic and Material Properties of used core Material.

Material	Thickness (mm)	Magnetic Permeability (Tesla)	Density (Kg/m^3)
M800-65A	0.65	2.383824512	7800
M-19	0.36	2.497142435	7600
M-43	0.64	2.815949276	7600
Pure soft Iron	0.11	3.536016114	7880
M890-50D	0.50	2.388282878	7850

Table 4. Comparison of Torque characteristics for different materials.

Materials	T_{max}	T_{min}	T_{avg}	T_{ripple}
M800-65A	6.56	1.06	3.85	1.42
M890-50D	3.94	0.73	2.43	1.317
M-43	3.88	0.74	2.39	1.311
M-19	3.69	0.69	2.31	1.29
Pure soft iron	4.15	0.813	2.504	1.33

3.1. Expression of core loss

(i) Method-I

The primary consideration of core loss is obtained as,

$$W_c = K.f^{\alpha}.B_m^{\beta} \tag{5}$$

W_c is the core loss,
f the field excitation frequency,
B_m maximum flux density,
K, α, β inferences the material parameters.

(ii) Method-II

The secondary consideration of estimating the core losses is segregated into hysteresis and eddy current losses as,

$$W_c = W_h + W_e \tag{6}$$

Where,

$$W_e = \frac{\sigma.\pi^2.d^2}{6.\rho}.B_m^2.f^2 \tag{7}$$

σ as conductivity, d is the thickness and ρ is the mass density of homogeneous laminating steel. Assuming, the hysteresis losses and skin effect are considered to be as negligible.

(iii) Method-III

The third consideration, in calculating the core losses can be,

$$W_c = W_h + W_e + W_{ex} \tag{8}$$

$$W_c = k_h f (B_m)^2 + K_e (f B_m)^2 + K_{ex} (f B_m)^{1.5} \tag{9}$$

Assuming K_h, K_e, K_{ex} are the coefficients of hysteresis loss, eddy current loss and excess loss respectively. So obviously the core losses are predicted by,

$$W_c = K_1 B_m^2 + K_2 B_m^{1.5} \tag{10}$$

$$K_1 = K_h f + K_e f^2 \tag{11}$$

$$K_2 = K_{ex} f^{1.5} \tag{12}$$

The calculation of core loss coefficient is obtained by,

$$K_e = \pi^2 \sigma \frac{d^2}{6} \tag{13}$$

Table 5. Core loss coefficients.

Material	K_h (W/kg)	K_e (W/kg)
M800-65A	0.0632	2.58e-5
M-19	0.02703	0.5e-6
M-43	0.0566	0.1e-6
Pure soft Iron	0.00012	0.23e-6
M890-50D	0.0517939	0.13e-6

K_1 And K_2 are obtained by minimizing the quadratic form,

$$f(K_1, K_2) = \sum[W_{ci} - (K_1 B_{mi}^2 + K_2 B_{mi}^{1.5})]^2 = \min \tag{14}$$

Considering W_{ci}, W_{mi} are the ith point of the data obtained from the curve of loss characteristics.

The coefficients of loss such as K_h, K_{ex} are obtained by,

$$K_h = \frac{(K_1 - K_e f_0^2)}{f_0} \tag{15}$$

$$K_{ex} = \frac{(K_2)}{f_0^{1.5}} \tag{16}$$

Where f_0 be the testing frequency of loss curve. The coefficients K_h and K_{ex} are estimated by using the curve of core loss data as in Table 5.

(iv) Method-IV

In another format the average core loss can be estimated by,

$$W_{cSRM} = \sum W_{cs}.m_s \tag{17}$$

The core loss and mass of steel for SRM are symbolled as W_{cs} and m_s respectively.

$$W_{cSRM} = P_{in} - P_{out} - W_{cu\_stator} - W_{cu\_rotor} - W_{mech} \tag{18}$$

The average core loss W_{cSRM} in the reluctance motor is correlated by obtaining output power of the shaft P_{out}, the copper loss W_{cu}, the mechanical losses W_{mech} and the input electric power P_{in}. The RMS value of current and the product with phase winding resistance is used to calculate the copper losses, assuming the IA, IB is the phase currents with each phase resistance as RA and RB.

$$W_{cu\_stator} = R_A I_A^2 + R_B I_B^2 \tag{19}$$

How over the absence of winding on the rotor create the copper loss as Zero indicated by,

$$W_{cu\_rotor} = 0 \tag{20}$$

The cross product of angular velocity and electromagnetic reluctance torque is considered to be as mechanical losses with 24.39W, 19.48128W, 19.31504W, 18.318W, 29.738W for M800-65A, pure soft iron, M890-50D, M-43 and M-19 respectively.

3.1.1. FEA Observations

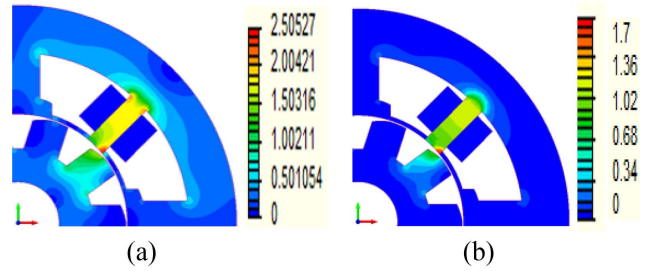The flux density distribution for different materials is

Fig. 24. (Color online) (a) Flux Density Distribution of SRM using M-19. (b) Hysteresis current loss distribution of SRM using M-19.
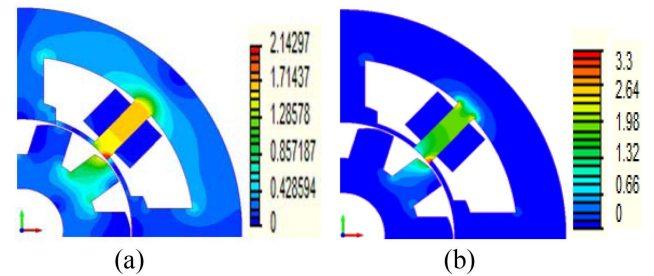

Fig. 25. (Color online) (a) Flux density distribution of SRM using M-43. (b) Hysteresis current loss of SRM using M-43.
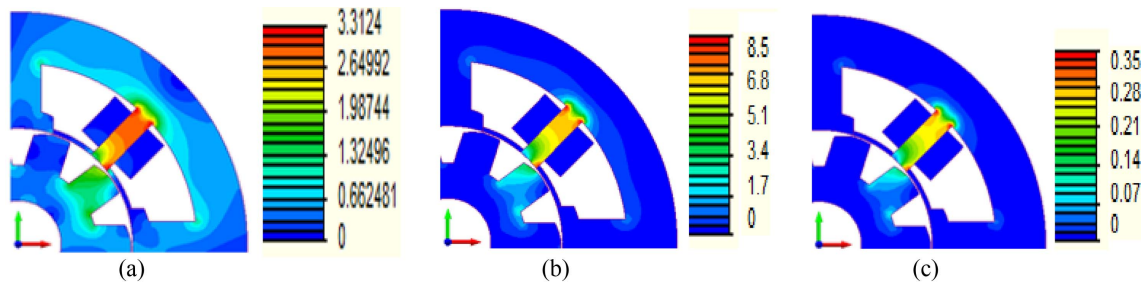

Fig. 23. (Color online) (a) Flux density distribution of SRM using M800-65A. (b) Hysteresis loss distribution of SRM using M800-65A. (c) Eddy current loss of SRM using M800-65A.
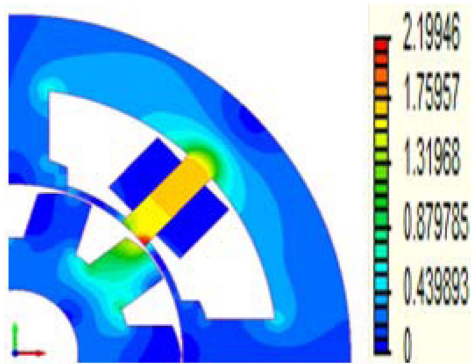
Fig. 26. (Color online) Magnetic flux density distribution of SRM using pure soft Iron.
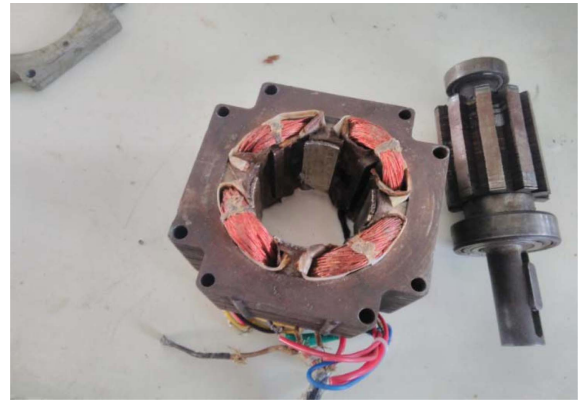

(a)   (b)

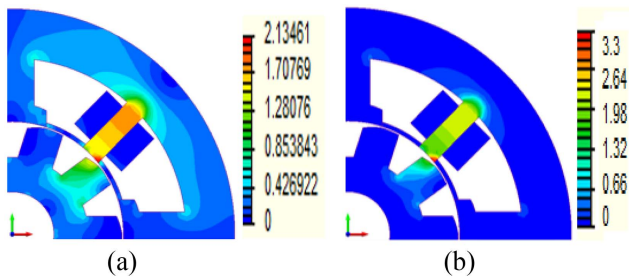**Fig. 27.** (Color online) (a) Flux density distribution of SRM using M890-50D. (b) Hysteresis current distribution of SRM using M890-50D.

Table 6. Comparison of Flux Density and corresponding losses for different materials.

Materials	Flux Density (Tesla)	Iron Losses (Watts)
M800-65A	3.3	8.85
M890-50D	2.13	3.3
M-43	2.14	3.3
M-19	2.5	1.7
Pure Soft Iron	2.19	0.001

shown in Figs. 23, 24, 25, 26 and 27 respectively and the corresponding loss values are tabulated in Table 6. From the table it is evident that the eddy current losses is negligible with M-43 and M890-50D. In case of Pure Soft Iron both hysteresis and Eddy current losses are negligible.

4. Prototype Implementation

The hardware validation is considered in two aspects. Namely, unexcited and excited condition.

(i) Unexcited condition
The cogging torque and Inductance are taken as the parameter for the valediction. Cogging torque is opposition

Fig. 28. (Color online) Prototype of the PM SRM.

Fig. 29. (Color online) Experimental setup for measuring cogging torque.

Table 7. FEA Vs Experimental Results.

Parameter	FEA	Experimental
Cogging Torque	0.197Nm	0.182Nm
Aligned Inductance	0.263H	0.29H
Unaligned Inductance	0.187H	0.11H

to reluctance torque. Figure 28 shows the geometry of PMSRM. The cogging torque is estimated by increasing the weights to machine until the condition varies. Figure 29 exhibits the experimental setup for cogging torque. Table 7 shows the comparability of FEA and Experimental Results for validations.

(ii) Excited Condition
The parameter under excited condition is taken as Acceleration, and Speed. The machine is excited with 1.5A of current for validation with FEA results. Figure 30 and Fig. 31 shows the experimental setup under the excitation condition for measuring accelerometer and current respectively. Figure 32 and Fig. 33 shows the current and voltage Waveform utilized for the excitation of PM-SRM.
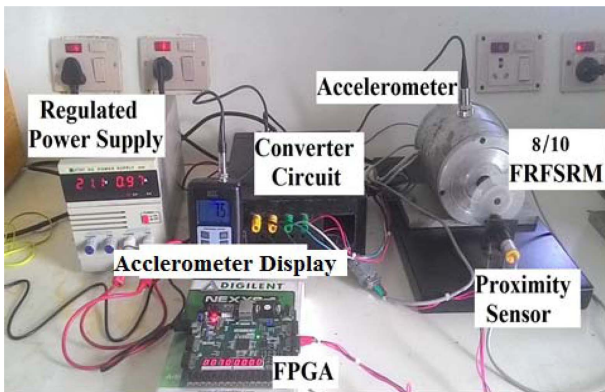
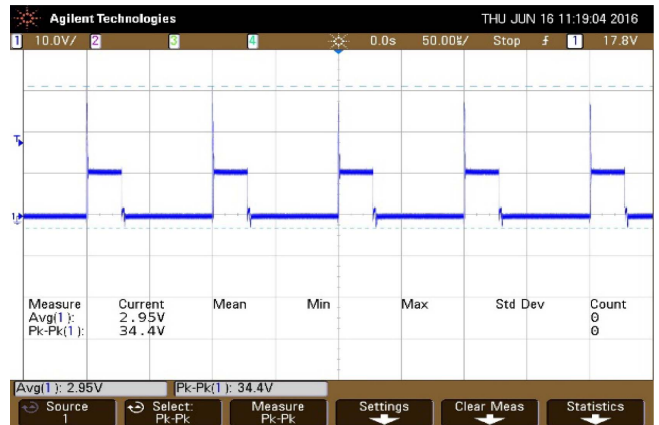**Fig. 30.** (Color online) Experimental setup for Acceleration in Deg/S².

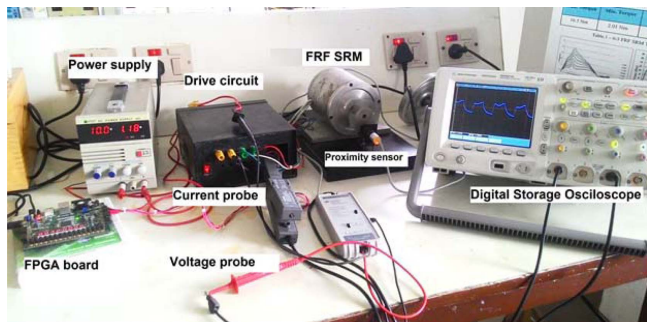**Fig. 31.** (Color online) Experimental setup for Speed, Voltage and Current measurements.

Fig. 32. (Color online) Current Waveform.

Table 8 compares the experimental and FEA results under excited condition.

Fig. 33. (Color online) Voltage waveform.

Table 8. Comparison of FEA and Experimental results under Excitation conditions.

Parameter	FEA	Experimental
Acceleration (Deg/S²)	70×10^4	75×10^4
Speed (rpm)	2100	2030

5. Conclusion

The effect in the orientation of PM in stator poles and choice of various laminating steel material on the performance of SRM has been examined by 2D FEA and by experimental study. Among the different permanent magnet orientation considered the PM Assists inter-linked stator pole configuration improves the average torque and air gap flux density. The cogging torque of this configuration is also minimum. Among the materials the M890-50D material has lower core losses. The future research work will be oriented towards vibration analysis, thermal analysis and torque ripple minimization.

Acknowledgments

Appendix 1

Table A. Specifications for the DSPM SRM.

References

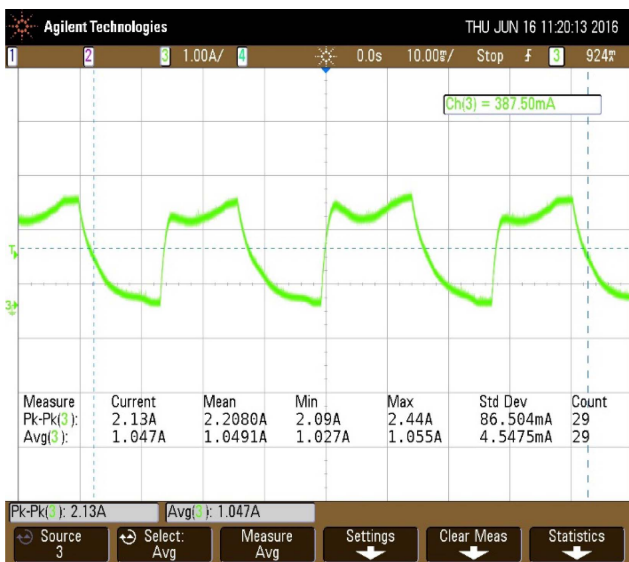[1] Lobo, Thesis Virginia polytechnic Institue and State Uni-

versity (2011).

[2] Cheewoo Lee, IEEE Trans. Ind. Appl. **45**, 703 (2009).

[3] S. Balamurugan, PhD-Thesis, Anna University, India (2009).

[4] R. Krishnan, IEEE Trans. Ind. Appl. **43**, 1247 (2007).

[5] V. Chandrasekar, PhD Thesis (2014).

[6] N. C. Lenin, PhD. Thesis, Anna University, India (2012).

[7] W. Fei, P. C. K. Luk, B. Xia, Y. Wang, and J. X. Shen, in Proceedings of IEEE Energy Conversion Congress and Exposition (ECCE), Atlanta, GA, USA (2010).

[8] Hamed Eskandari and Mojtaba Mirsalim, IEEE Trans. Energy Conversion **28**, (2013).

[9] Z. Q. Zhu and David Howe, IEEE Trans. Energy Conversion **15**, 407 (2000).

[10] Jisha Kuruvila, Abhijit P., Mathew Jacob, Ramesh Babu, Swathy Mohan V., and Varun Jo Abu, IJAREEIE **4**, 4 (2015).

[11] T. J. E. Miller, Brushless Permanent Magnet and Reluctance Motor Drives, Clarendon Press, Oxford (1989) pp 58-62.

[12] Praveen Vijayraghavan, Ph.D. Thesis, Virginia Polytechnic Institute and State University, Blacksburg, Virginia (2001).

[13] Md Ashfanoor Kabir and Iqbal Husain, in Proceedings of Energy Conversion Congress and Exposition, Milwaukee, WI, USA (2016).

[14] Chun Gan, Jianha Wu, Mengjie Shen, Shiyou Yang, Yihua Hu, and Wenping Cao, IEEE Trans. Magn. **51**, 9 (2015).

[15] Yusuf Ozoglu and Nurdan Guzelbeyoglu, in Proceedings of International Conference on Electrical and Electronics Engineering (ELECO), Turkey (1999) pp 305-308.

[16] Yu Chen, Z. Q. Zhu, and David Howe, IEEE Trans. Ind. Appl. **44**, 6 (2008).

[17] J. Kartigeyan and M. Ramaswamy, J. Magn. **22**, 93 (2017).

Table A. Specifications for the DSPM SRM.

Description	Symbol	Value
Number of stator main poles	Ns	4
Number of shared pole	Ncp	4
Number of rotor poles	Nr	10
Power output	P	0.55 kW
Voltage	V	500 V
Speed	N	2800 rpm
Stator main pole arc	βs	11.5°
Stator shared pole arc	βcp	36°
Rotor pole arc	βr	19°
Outer stator diameter	Do	53.25 mm
Stator back iron thickness	C	11.65 mm
Bore diameter	D	54.1 mm
Rotor pole tip diameter	Dro	52.6 mm
Rotor pole bottom diameter	Dri	36.4 mm
Air gap (Main Pole)	g1	0.75 mm
Air gap (Shared Pole)	g2	0.3 mm
Shaft diameter	Dsh	20 mm
Height of main stator pole	hs	15 mm
Height of rotor pole	hr	8.26 mm
Height of shared stator pole	hcp	10.53 mm
Length of the permanent magnet	lm	1 mm
Width of shared pole	Wcp	10.66 mm
Inner radius of shared pole	Rsp	26.6 mm
Height of shared pole-pole shoe	hspp	2.75 mm
Stack length	L	60 mm
Peak current	Ip	1.1 A
Permanent magnet material		NdFeB
Lamination material		CR10